3-2022

Determination of Vortex Locations in a 2x2 Array of Josephson Junctions for Topological Quantum Computation

Casey L. Kowalski

DETERMINATION OF VORTEX LOCATIONS IN A 2X2 JOSEPHSON JUNCTION ARRAY FOR TOPOLOGICAL QUANTUM COMPUTATION

THESIS

Casey L. Kowalski, 2Lt, USAF

AFIT-ENP-MS-22-M-099

AFIT-ENP-MS-22-M-099

Determination of Vortex Locations in a 2x2 Josephson Junction Array for

Topological Quantum Computation

THESIS

Presented to the Faculty

Department of Engineering Physics

Graduate School of Engineering and Management

Air Force Institute of Technology

Air University

Air Education and Training Command

in Partial Fulfillment of the Requirements for the

Degree of Master of Science in Applied Physics

Casey L. Kowalski, B.S.

2Lt, USAF

March 24, 2022

Determination of Vortex Locations in a 2x2 Josephson Junction Array for

Topological Quantum Computation

THESIS

Casey L. Kowalski, B.S.
2Lt, USAF

Committee Membership:

Michael V. Pak, Ph.D.
Chair

Anil K. Patnaik, Ph.D.
Member

David E. Weeks, Ph.D.
Member

AFIT-ENP-MS-22-M-099

Abstract

A large barrier to practical quantum computation exists in the form of qubit decoherence, which leads to high noise and error when implementing quantum algorithms. A potential solution to this problem is the use of topologically-protected Majorana-based qubits, as their nonlocal nature and unique non-abelian exchange statistics render them virtually immune to decoherence while still allowing the state to be easily manipulated. For such a qubit to be constructed, it is essential to know the locations of the Majorana-hosting vortices in the system. This work presents a solution for the formation locations of vortices in a 2x2 superconducting island array, paving the way for the analysis of larger arrays that allow for the physical exchange of particles. Additionally, a method for determining the vortex locations in an irregularly-shaped Josephson junction is derived, allowing for accurate predictions of Majorana fermion locations in manufactured systems where the junctions may not be perfectly straight.

Table of Contents

List of Figures

I. Introduction

The field of quantum computing is currently plagued by decoherence, a quantum system's tendency to interact with the environment, which alters the state of the system. Decoherence in a qubit results in noise when one attempts to run algorithms on a quantum computer and is an issue that affects every qubit system to date. In fact, it is such a problem that the largest number to be successfully factored by Shor's prime factorization algorithm is only 21 (1). While there are error correction methods available, the decoherence time of the qubit must be $10^4 - 10^5$ times higher than the time it takes to perform a single gate operation for them to be successful (2). Because of this, recent interest has arisen in Majorana-based qubits, which are very resistant to decoherence. These qubits consist of highly nonlocal zero-energy excitations of the ground state and provide topological protection for the system, which means local perturbations do not affect the Hamiltonian eigenstates of the system. Since almost all sources of decoherence are local perturbations, implementation of Majorana-based qubits could allow for successful application of error correction techniques, or even eliminate the need for them altogether.

While these topological qubits exhibit great potential, the theory behind them must be fleshed out more if they are going to be successfully constructed and implemented. Producing a system that can host Majorana fermions for use in quantum computation is an ongoing area of research. Majorana fermions cannot exist in common s-wave superconductors, as it is necessary for the superconductor to exhibit p-wave pairing in order to host them. However, it is known that a topological insulator where superconductivity has been induced by a nearby superconductor can exhibit the necessary material properties to host the Majorana fermions in vortex cores located on its surface (3). What is not known, however, is where these vortex cores will form for various system configurations. Knowledge of the vortex locations is

essential to the construction of a qubit because the state of the system is manipulated by moving the Majorana fermions around each other.

Vortices are known to exist in a Josephson junction, and as such, a promising candidate for a Majorana-based qubit involves an array of superconducting islands placed on a topological insulator. This array will create a series of Josephson junctions, each containing a number of vortices. Application of a voltage between two islands can move the vortices within the junction, and when applied to an array, can allow for vortices to be moved around each other as needed for quantum gate implementation. Such movement of vortices would be analogous to automobiles driving around a city block, with the street representing the Josephson junction, and would provide a method of hands-free qubit manipulation. However, exact vortex locations for this configuration are not well known and additionally, the manufacture of such arrays can result in irregularly shaped Josephson junctions, posing a problem for experimental implementation based off the existing literature.

This work seeks to provide insight to such systems and exists as a standalone review, although an understanding of quantum mechanics and a basic knowledge of second quantization are recommended. It begins with a brief review of the relevant superconducting theory including the superconducting wavefunction and the idea of quantized magnetic flux. This is followed by a basic explanation of what Majorana fermions are and the exchange statistics that allow them to be used to form a qubit. Next, the Josephson junction is introduced as well as the concept of vortices and where they exist in a basic junction. These concepts are then expanded to include an irregularly shaped junction, so that in laboratory implementations where the junctions are not perfectly straight, researchers are able to more accurately predict the formation locations of the vortices. Finally, a 2x2 array of superconducting islands is presented and analyzed for vortex formation locations. While a 2x2 array is not

large enough to allow for particle exchange, it paves the way for larger arrays that can do so, as the concepts presented can simply be expanded to include more islands and thus more Josephson junctions.

II. Background

The purpose of this chapter is to develop a basic understanding of the superconducting theory required for this work in addition to an introduction to Majorana states and their potential utilization in quantum computing. First, the basic concepts of superconductivity are presented via a summary of London theory. Subsequently, the concept of Majorana fermions and zero-enegy modes are introduced and related to quantum computing. The chapter will then move to a derivation of the Josephson junction and a treatment of a basic, straight-walled junction to predict vortex locations.

2.1 London Theory

London theory is a treatment of superconductors created by Fritz and Heinz London in 1935 (4). The equations it presents are derived from observed superconducting phenomena, and although BCS theory is the most complete treatment of superconductors, London theory will suffice for the basic knowledge of superconducting theory required for this work. Without going into full derivations, this section lays out the relevant aspects of superconductors for this work. If a complete derivation of London theory is desired, reference (5).

In the early 1900s, it was observed that some metals, when cooled past certain critical temperatures near absolute zero, abrubtly exhibited zero electric resistance. This led physicists at the time to assume the existance of some complex, electrically charged bosonic field which falls into the ground state at the observed critical temperature. For a homogeneous superconductor, meaning the bosonic number density is constant, this field is given by

$$\Psi(\mathbf{r}, t) = \sqrt{n_B} e^{i\phi(\mathbf{r},t)}, \tag{1}$$

where Ψ is the value of the bosonic field at position $\mathbf{r}$ and time t, n_B is the bosonic number density, and ϕ is the superconducting phase. The charge quantum q of the bosonic field was found to be

$$q = 2e, \tag{2}$$

where e is the charge of an electron. Therefore, the field is comprised of pairs of electrons, called cooper pairs.

One important characteristic of superconductors is the ability to screen magnetic fields, called the Meissner effect. This essentially states that a magnetic field $\vec{B}$ will be screened to zero in the bulk of a superconductor, even if the field exists before the metal is brought down past its critical temperature. This screening happens within a characteristic distance λ_L from the surface of the superconductor. λ_L is given by

$$\lambda_L = \sqrt{\frac{m_B}{n_B \mu_0 q^2}}, \tag{3}$$

where $m_B = 2m_e$ is the mass of a cooper pair and μ_0 is the chemical potential of the boson field, and is called the London penetration depth.

Consider a magnetic flux Φ contained by a superconducting ring, as shown in Figure 1. If a contour C is defined within the ring beyond the London penetration depth, the magnetic field along C is zero via the Meissner effect. The second London equation reads

$$\frac{\partial}{\partial r} \times (\Lambda \mathbf{j}_s) = -\mathbf{B}, \tag{4}$$

where $\Lambda = \frac{m_B}{n_B q^2}$. This means that zero magnetic field results in zero supercurrent along the contour. Subsequently, the first London equation,

$$\frac{\partial (\Lambda \mathbf{j}_s)}{\partial t} = \mathbf{E}_{eff}, \tag{5}$$
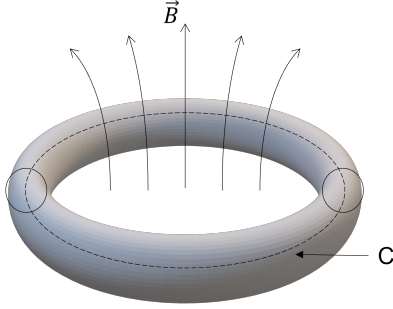
Figure 1. Magnetic flux through a superconducting ring.

shows that, in this case, the effective electric field $\mathbf{E}_{eff} = \mathbf{E} = 0$ as well. The time derivative of the flux through the contour, via the integral form of Faraday's law, is

$$\frac{d\Phi}{dt} = -\oint_C \mathbf{E} \cdot d\mathbf{l} = 0. \tag{6}$$

This means that the magnetic flux through the superconducting ring is trapped, even if the applied field is varied in time.

The supercurrent density is related to the superconducting phase gradient and vector potential $\vec{A}$ by the relation

$$\Lambda \mathbf{j}_s = \frac{\hbar}{q} \frac{\partial \theta}{\partial \mathbf{r}} - \mathbf{A}. \tag{7}$$

Since $\vec{j_s} = 0$ along the contour,

$$\mathbf{A} = \frac{\hbar}{q} \frac{\partial \theta}{\partial \mathbf{r}}. \tag{8}$$

Integrating along the contour and using Stokes' theorem in conjunction with $\nabla \times \vec{A} =$

$\vec{B}$ yields

$$\oint_C \mathbf{A} \cdot d\mathbf{l} = \Phi = \frac{\hbar}{q} \oint_C \frac{\partial \theta}{\partial \mathbf{r}}. \tag{9}$$

The integral of the phase gradient around the contour represents the total phase change, and thus must be equal to an integer multiple n of 2π in order for the wavefunction to be unique. Therefore, Equation 9 becomes

$$\Phi = \frac{\hbar}{q} 2\pi n. \tag{10}$$

Equation 10 introduces the concept that flux through a superconducting ring is quantized, with the fundamental flux quantum defined as

$$\Phi_0 = \frac{h}{2e}. \tag{11}$$

The flux quantum is an important concept to understand, as it will determine the number of Josephson vortices, and thus Majorana zero modes, contained in a Josephson junction, which is discussed later. Additionally, it is related to Abrikosov vortices by the fact that an Abrikosov vortex is a location where exactly one quantum of magnetic flux punctures a superconducting region. This results in a circulation of supercurrent around this location, analogous to a superconducting ring.

2.2 Majorana Fermions

Increasing qubit decoherence time persists as one of the most important problems to be solved in the area of quantum computing. Majorana-based qubits are a promising solution to this problem, as their nonlocal nature causes them to be inherently resistant to local perturbations, thus dramatically increasing their decoherence times (6). The following description of Majorana zero modes is based on the paper by

Leijnse and Flensberg (7).

A Majorana fermion (MF) is an anyonic particle which is its own antiparticle, meaning its creation operator is equal to its annihilation operator, $\gamma^\dagger = \gamma$. The qubit potential for MFs comes from their non-abelian exchange statistics: particle exchange is a nontrivial operation, and the state of a system can be altered via swapping, or braiding, particles. Any normal fermion can be defined as a superposition of two MFs, where one MF represents the real component of the fermion, and the other MF represents the imaginary component. This is true even when the two MFs are spatially separated, and this spatially separated case is what gives them applicability to quantum computing in the form of manipulation of Majorana zero modes.

Kitaev Chain.

The most basic understanding of a Majorana zero mode in a p-wave superconductor comes from the example of the Kitaev 1D tight-binding chain. This consists of a chain of N individual sites which can contain either 1 or 0 electrons with chemical potential μ. Site i can only interact with its immediate neighbors, sites $i-1$ and $i+1$. The hopping t denotes the energy required to move an electron from one occupied site to an adjacent unoccupied site and is analogous to kinetic energy. The superconducting gap Δ represents pairing energy from two adjacent occupied or unoccupied sites. The Hamiltonian of the chain is given by

$$H_{chain} = -\mu \sum_{i=1}^{N} n_i - \sum_{i=1}^{N-1} \left(t c_i^\dagger c_{i+1} + \Delta c_i c_{i+1} + h.c. \right), \tag{12}$$

where $c_i^\dagger$ (c_i) is the creation (annihilation) electron operator on site i, $n_i = c_i^\dagger c_i$ is the electron number operator, and $h.c.$ denotes the hermetian conjugate.

Since each electron in the chain can be defined by two MFs, it is possible to rewrite the electron creation and annihilation operators in terms of these Majorana opera-

tors, with $\gamma_{i,1}$ representing the real component and $\gamma_{i,2}$ representing the imaginary component of the electron. The top portion of Figure 2 displays the chain and the redefinition of electrons into MFs. Doing this transforms the operators according to

$$c_i = \frac{1}{2} \left(\gamma_{i,1} + i\gamma_{i,2} \right), \tag{13}$$

$$c_i^\dagger = \frac{1}{2} \left(\gamma_{i,1} - i\gamma_{i,2} \right). \tag{14}$$

Setting $\mu = 0$ and $\Delta = t$ for simplicity and plugging Equations 13 and 14 into Equation 12, the Hamiltonian becomes

$$H = -it \sum_{i=1}^{N-1} \gamma_{i,2}\gamma_{i+1,1}. \tag{15}$$

Because it is possible to define any fermion as a superposition of two MFs, a new fermion operator $\tilde{c}_i$ can be defined by grouping together MFs of neighboring sites, such that

$$\tilde{c}_i = \frac{1}{2} \left(\gamma_{i+1,1} + i\gamma_{i,2} \right). \tag{16}$$

This new grouping is shown in the bottom portion of Figure 2. Rewriting the Hamiltonian in terms of $\tilde{c}_i$ and $\tilde{c}_i^\dagger$, we obtain

$$H = 2t \sum_{i=1}^{N-1} \tilde{c}_i^\dagger \tilde{c}_i. \tag{17}$$

Using these newly redefined fermions is really just a way to diagonalize Equation 12, and while it is helpful for organization of thought, the important physics take place in Equation 15. Upon inspection, it is observed that the MF operators $\gamma_{1,1}$ and $\gamma_{N,2}$ are not included in the Hamiltonian, and are thus completely decoupled from the energy of the system. A new operator $\tilde{c}_m$ can be defined from these two
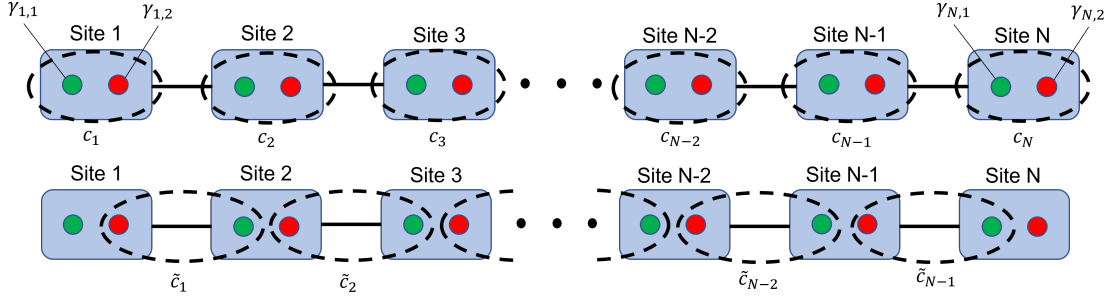
9

Figure 2. (Top) The 1D tight binding chain with fermionic electron operators c_i represented as a grouping of two MF operators. The MF representing the real component of the electron is green and denoted by $\gamma_{i,1}$, while the MF representing the imaginary component is red and given by $\gamma_{i,2}$. (Bottom) The same chain, but with new fermion operators $\tilde{c}_i$ defined to contain MFs from neighboring site. This leaves an unpaired MF on either end of the chain, which are grouped together to define the nonlocal fermion operator $\tilde{c}_m$.

MFs according to

$$\tilde{c}_m = \frac{1}{2}\left(\gamma_{1,1} + i\gamma_{N,2}\right). \tag{18}$$

This new operator represents a fermionic state which is highly nonlocal, and the occupation of which has no impact on the energy of the system. This quasiparticle gives the system a doubly degenerate ground state which is highly resistant to local perturbations, and is referred to as a Majorana zero mode.

Unfortunately, not all superconductors have the ability to host Majorana zero modes. In order for Majorana zero modes to exist, the superconductor must be in a topologically nontrivial state, which is where the chemical potential satisfies the relation $|\mu| < 2t$. The Majorana zero modes form at the boundaries of these topological regions, so if the Kitaev chain has sections where $|\mu| > 2t$, more Majorana fermions will appear at the points where the system switches from a topological to a non-topological state.

The Hamiltonian in Equation 12 can be expanded to a continuous two-dimensional

case. The Hamiltonian for this continuous 2D p-wave superconductor is

$$H_{2D}^{pw} = \int d^2r \left[\Psi^\dagger(\mathbf{r}) \left(\frac{\mathbf{p}^2}{2m} - \mu \right) \Psi(\mathbf{r}) + \Psi(\mathbf{r})|\Delta|e^{i\phi}(p_x \pm ip_y)\Psi(\mathbf{r}) + h.c. \right], \quad (19)$$

where $\mathbf{p}$ is momentum, m is the electron mass, and $\Psi^\dagger$ is the real-space creation operator. As the Majorana zero modes exist at the ends of the wire in the case of the Kitaev chain, in two dimensions they form at similar boundary points, namely at the cores of Abrikosov and Josephson vortices, as these represent places where superconductivity is broken (8).

While actual superconductors with the correct material properties to satisfy the topological non-triviality requirements are exceedingly rare, a class of materials known as topological insulators (TIs) exhibit promise. Although not superconductors in their own right, they can be induced into a superconducting state by placing an actual superconductor on top of them, as shown in Figure 3. This happens due to the wavefunction of the cooper pairs from the superconductor slightly penetrating the topological insulator and coupling into its Hamiltonian. By adjusting the geometry of

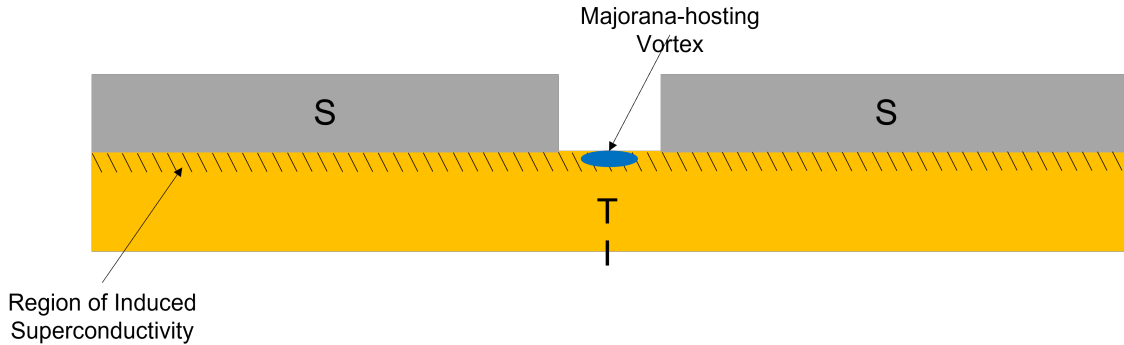**Figure 3. Induced Layer of Superconductivity on a Topological Insulator. The two superconductors (gray) placed onto a topological insulator (orange) induce a state of superconductivity in the TI. Creating a vortex (blue) on the surface of this induced layer produces a region with the right material properties to host a Majorana zero mode.**

the superconductors, the superconducting properties of the topological insulator can

be manipulated to force them into a topologically non-trivial state (9). Therefore, boundary points to the induced superconducting region, i.e. vortex cores created on the surface of the TI, will have the ability to host Majorana zero modes. It is the goal of this work to predict where these vortices form so that they may be used to help realize an error-resistant topological qubit.

Exchange Statistics.

The unique non-abelian exchange statistics of Majorana states provides the mechanisms with which they can be used to implement quantum gates. For a wavefunction given by the tensor product of two identical particle states $|\psi\rangle$ and $|\phi\rangle$, the exchange operator P acting on the state results in the original wavefunction multiplied by $+1$ for bosons and -1 for fermions, such that

$$P_{boson} |\psi\rangle |\phi\rangle = |\phi\rangle |\psi\rangle = |\psi\rangle |\phi\rangle , \tag{20}$$

$$P_{fermion} |\psi\rangle |\phi\rangle = - |\psi\rangle |\phi\rangle . \tag{21}$$

If the particles being exchanged are two-dimensional anyons that obey normal abelian statistics, the wave function is transformed by an overall phase factor θ according to

$$P_{albelian} |\psi\rangle |\phi\rangle = e^{i\theta} |\psi\rangle |\phi\rangle . \tag{22}$$

For non-abelian anyons, particle exchange will actually send the system into a different state instead of introducing a phase shift. This can be best understood by a system of three particles, $|\psi\rangle = |\psi_1\rangle |\psi_2\rangle |\psi_3\rangle$. If particles 1 and 2 are exchanged, the transformation is represented by $|\psi'\rangle = U_{1,2} |\psi\rangle$, with $U_{\alpha,\beta}$ being a 3x3 unitary matrix. Exchange of particles 2 and 3 is represented by $|\psi'\rangle = U_{2,3} |\psi\rangle$, and if $U_{1,2}$ does not commute with $U_{2,3}$, the particles obey non-abelian statistics (10). For this

condition to be met, the system must have two degenerate states, which in the case of this work, are the two degenerate ground states brought about by the existance, or lack thereof, of a Majorana zero mode.

To make sense of how these exchange statistics operate, imagine two spatially separated vortices on a plane, as shown in Figure 4. The superconducting phase
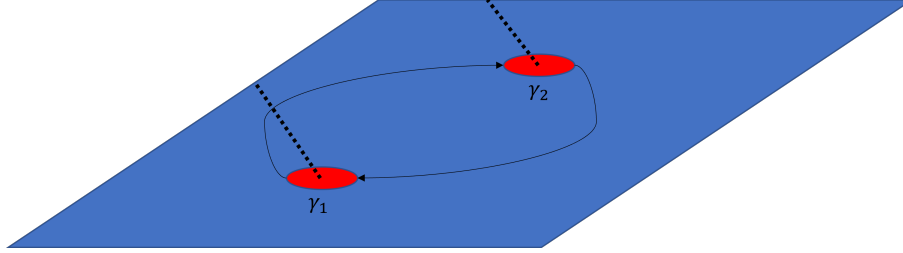

Figure 4. The exchange described by the braiding operator B_{12}. As vortex 1 passes behind vortex 2, it crosses its branch cut (dotted line), thus picking up a phase shift of π.

winds by 2π around a vortex, but an imaginary line called a branch cut can be defined that extends radially outward from each vortex in one direction, such that the superconducting phase is constant except for at the branch cut, where it jumps by 2π. The directions of the branch cuts are arbitrary, but it is simpler to have them all facing the same direction. Whenever one vortex crosses another's branch cut, it receives a phase shift of 2π; however, since the MF operator contained in the vortex is essentially half of a normal fermion, it receives a phase shift of π. Imagine now that vortex 1 and vortex 2 are exchanged such that vortex 1 passes over the branch cut of vortex 2 and acquires a phase shift of π, but vortex 2 does not. This exchange is shown by the arrows in Figure 4, and results in the MF operator transformations

$$\gamma_1 \rightarrow -\gamma_2, \tag{23}$$

$$\gamma_2 \rightarrow +\gamma_1. \tag{24}$$

In this transformation, the subscripts on the operator refer to the positions of the

vortices relative to one another: γ_1 becomes $-\gamma_2$ because it now occupies the location 2 and acquired the phase shift of π from passing over vortex 2's branch cut. This particular transformation forms the basis for constructing quantum gates and is called the braid operator B_{12} such that

$$\gamma_i \rightarrow B_{12}\gamma_i B_{12}, \tag{25}$$

where

$$B_{12} = \frac{1}{\sqrt{2}}\left(1 + \gamma_1\gamma_2\right). \tag{26}$$

It is important to note that in order to use the branch cut technique to describe the exchange statistics, the vortices must be completely exchanged, that is, the final location of vortex 2 must be the initial location of vortex 1, and vice versa.

Unfortunately, braiding with just two MF particles is not sufficient to change the state of the system in the number basis. After such an exchange, measuring the fermionic number operator by bringing the two MFs together will result in the same state the system was previously in. To be precise, the effects that the braid operator has when acting on the number states are

$$B_{12}\left|0\right\rangle = \frac{1}{\sqrt{2}}\left(1 + i\right)\left|0\right\rangle, \tag{27}$$

$$B_{12}\left|1\right\rangle = \frac{1}{\sqrt{2}}\left(1 - i\right)\left|1\right\rangle. \tag{28}$$

If four MFs are used, however, the non-abelian statistics can work to change the state. For such a system, measurement of fermion 1 is comprised of combining MFs 1 and 2, and measurement of fermion 2 by combining MFs 3 and 4. Operating with B_{12} and B_{34} will only result in an overall phase factor like in the two MF case, but braiding

MFs 2 and 3 will result in a superposition of the states $|00\rangle$ and $|11\rangle$ given by

$$B_{23}|00\rangle = \frac{1}{\sqrt{2}}\left(|00\rangle + i|11\rangle\right), \tag{29}$$

$$B_{23}|11\rangle = \frac{1}{\sqrt{2}}\left(|11\rangle - i|00\rangle\right). \tag{30}$$

Since this system of four MFs can be manipulated from one state to another by braiding, it can be used to define a qubit with a computational basis set of $|\tilde{0}\rangle = |00\rangle$ and $|\tilde{1}\rangle = |11\rangle$.

With individual qubits comprised of only 4 MFs, the qubit is limited to rotations of $\pi/2$ on the Bloch sphere and entanglement is impossible, so in order to implement the myriad of gates used in quantum computing, more complex qubits must be defined. In 2007, Georgiev described how two overlapping four-MF qubits can be braided to generate entanglement in the form of a CNOT gate (11). This overlapping qubit concept is shown in Figure 5. Additionally, Hassler et al. discusses combin-
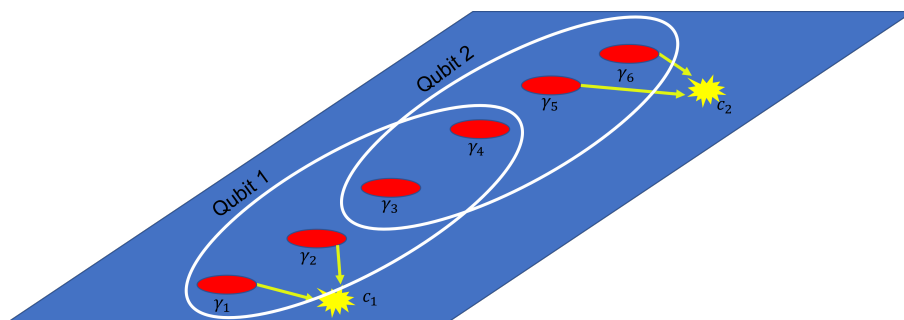

Figure 5. A concept of two overlapping MF qubits to generate entanglement. The MFs encircled in white comprise each respective qubit. The state of qubit 1 is found by measuring the fermion associated with γ_1 and γ_2, while γ_5 and γ_6 comprise the state of qubit 2, as shown in yellow (11).

ing Majorana bound states with a flux qubit to explore more of the Hilbert space while maintaining the topological protection provided by non-abelian anyons (12). It is therefore possible, with innovative qubit designs, to surmount the restrictions imposed by the braiding of four MFs alone.

2.3 Josephson Junctions

Physical analogues for the ends of a Kitaev chain are exceedingly rare. Currently, the best known system is comprised of the boundaries of a superconducting region on the surface of a topological insulator, where superconductivity has been induced by an actual superconductor (3). These boundaries are associated with points on the topological insulator where the superconducting gap Δ goes to zero, meaning superconductivity is broken. This occurs at the cores of Abrikosov and Josephson vortices, the latter of which is explained in this section.

In 1962, Brian David Josephson predicted the tunneling of supercurrent between two superconductors separated by a small, insulated gap (13)(14). Since then, the Josephson Junction has found many applications in the field of physics. The ability to use them to construct superconducting quantum interference devices (SQUIDs) has led to the many types of state-of-the-art transmon qubits that currently dominate the world of quantum computing (15)(16). Josephson Junctions are critical to this work because they harbor the potential to host and manipulate Majorana zero modes, which can be used to define a qubit. Therefore, a basic understanding of the physics behind Josephson Junctions is necessary.

In order to derive the fundamental current relationship across a Josephson junction, first consider two identical superconductors separated by a thin, insulating layer, as shown in Figure 6 (15). The wavefunctions of cooper pairs for each superconductor
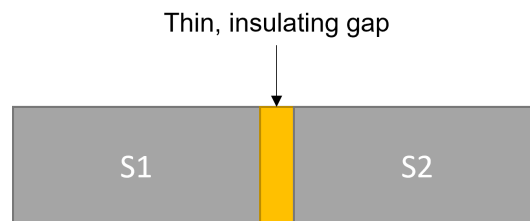

Figure 6. A Josephson junction, consisting of two identical superconductors S_1 and S_2 separated by a thin, insulating gap.

are given by Equation 1, and are weakly coupled by coupling constant K due to their spatial proximity. The system is governed by two Schrödinger equations,

$$i\hbar\frac{\partial\Psi_1}{\partial t} = E_1\Psi_1 + K\Psi_2, \tag{31}$$

$$i\hbar\frac{\partial\Psi_2}{\partial t} = E_2\Psi_2 + K\Psi_1, \tag{32}$$

where K is a constant representing the weak coupling between the superconductors due to cooper pair tunneling, and $E_{1,2}$ are the electric potentials of the respective superconductors. If a voltage V is applied between the superconductors, and the zero energy reference is defined to be directly between them, E_1 and E_2 become $+\frac{qV}{2}$ and $-\frac{qV}{2}$, respectively, where $q = 2e$ is the charge of the cooper pairs. Plugging in the respective wavefunctions, the Schrödinger equations become

$$-\hbar\sqrt{n_1}\frac{\partial\phi_1}{\partial t} + \frac{i\hbar}{2\sqrt{n_1}}\frac{\partial n_1}{\partial t} = \frac{qV}{2}\sqrt{n_1} + K\sqrt{n_2}e^{i(\phi_2-\phi_1)}, \tag{33}$$

$$-\hbar\sqrt{n_2}\frac{\partial\phi_2}{\partial t} + \frac{i\hbar}{2\sqrt{n_2}}\frac{\partial n_2}{\partial t} = -\frac{qV}{2}\sqrt{n_2} + K\sqrt{n_1}e^{i(\phi_1-\phi_2)}. \tag{34}$$

Expanding the exponential according to Euler's identity and separating real and imaginary components yields the four equations

$$\frac{\hbar}{2\sqrt{n_1}}\frac{\partial n_1}{\partial t} = K\sqrt{n_2}\sin(\phi_2-\phi_1), \tag{35}$$

$$\frac{\hbar}{2\sqrt{n_2}}\frac{\partial n_2}{\partial t} = K\sqrt{n_1}\sin(\phi_1-\phi_2), \tag{36}$$

$$-\hbar\sqrt{n_1}\frac{\partial\phi_1}{\partial t} = \frac{qV}{2}\sqrt{n_1} + K\sqrt{n_2}\cos(\phi_2-\phi_1), \tag{37}$$

$$-\hbar\sqrt{n_2}\frac{\partial\phi_2}{\partial t} = -\frac{qV}{2}\sqrt{n_2} + K\sqrt{n_1}\cos(\phi_1-\phi_2). \tag{38}$$

17

From Equation 35 and Equation 36, it can be seen that $\frac{\partial n_1}{\partial t} = -\frac{\partial n_2}{\partial t}$. By defining the current $I = \Omega q \frac{\partial n}{\partial t}$, where Ω is the superconductor volume, it is evident that this means any current leaving S_1 is equal to the current entering S_2. Additionally, by defining $n_1 = n_2 = n$, we can reduce Equation 35 to

$$I_s = I_c \sin\left(\phi_2 - \phi_1\right) = I_c \sin \Delta\phi, \tag{39}$$

where $I_c = 2Knq\Omega/\hbar$ is the maximum amount of current that can tunnel through the junction and is called the critical current. Equation 39 is known as the first Josephson relation, and it shows that a phase difference between the two superconductors will result in current across the junction. Importantly, when $\Delta\phi = m\pi$ with $m = 0, 1, 2, ...,$ current does not flow. Additionally, it is important to note that this current is not the result of any applied voltage; it is solely due to a difference in the superconducting phase between the two superconductors.

Subtracting Equation 37 from Equation 38 yields the second Josephson relation,

$$\frac{\partial}{\partial t}\left(\phi_2 - \phi_1\right) = \frac{qV}{\hbar}, \tag{40}$$

which describes how an applied voltage will cause the phase difference across the gap to evolve in time.

In the presence of a magnetic field, Equation 39 and Equation 40 must be altered to be gauge invariant. This is done by replacing $\Delta\phi$ with the gauge invariant phase γ, which is given by the transformation

$$\Delta\phi \to \gamma = \phi_2 - \phi_1 + \frac{2\pi}{\Phi_0}\int_1^2 \vec{A}\cdot d\vec{s}, \tag{41}$$

where the integration is taken across the insulating gap (17). This transforms the

first and second Josephson relations to

$$I = I_c \sin \gamma, \tag{42}$$

$$\frac{\partial}{\partial t}\gamma = \frac{qV}{\hbar}. \tag{43}$$

Consider now a Josephson junction of finite length l and width d in the presence of a uniform magnetic field oriented perpendicular to the plane, as shown in Figure 7. The superconductors screen the magnetic field such that no field penetrates their
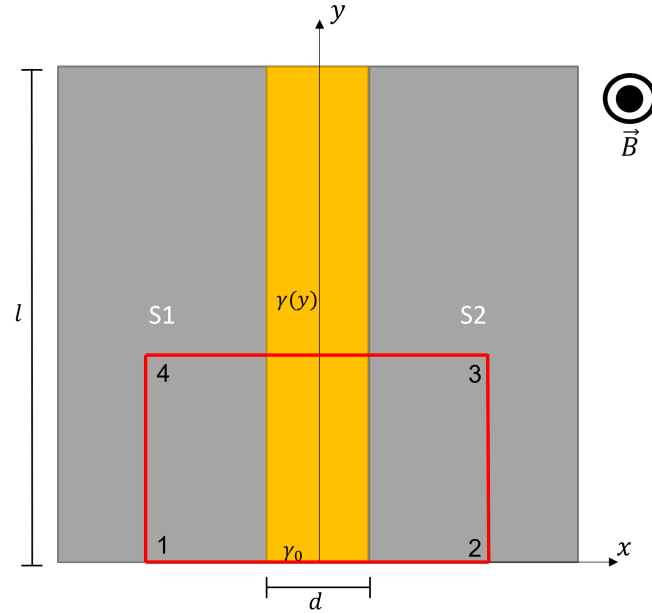

Figure 7. Top-down view of a Josephson junction of finite length and width in a uniform Magnetic field oriented perpendicular to the plane.

bulk, allowing for only the field penetrating the insulating gap to be considered. If $\gamma(0) = \gamma_0$ at the base of the junction, it is possible to find γ an arbitrary distance y farther up the junction by examination of the magnetic flux. The flux Φ within the area contained by the box is related to the vector potential $\vec{A}$ by

$$\Phi = Byd = \oint \vec{A} \cdot d\vec{s}, \tag{44}$$

19

where the integral is taken along the outside of the box, leading to

$$Byd = \int_1^2 A_x dx + \int_2^3 A_y dy + \int_3^4 A_x dx + \int_4^1 A_y dy. \tag{45}$$

Since the superconductors screen the field from their bulk, if the contours $2 \to 3$ and $4 \to 1$ are defined to be farther into the superconductors than the London penetration λ, the vector potential is approximately equal to zero along their length. This allows the second and fourth integrals in Equation 45 to vanish. If the gauge is subsequently chosen to be $A_x = -By$ and $A_y = 0$, the first integral also vanishes and Equation 45 becomes

$$Byd = \int_3^4 A_x dx. \tag{46}$$

The gauge invariant phases across the gaps are, from Equation 41,

$$\gamma(0) = \phi_2 - \phi_1 = \gamma_0, \tag{47}$$

$$\gamma(y) = \gamma_0 + \frac{2\pi}{\Phi_0} \int_3^4 A_x dx = \gamma_0 + \frac{2\pi}{\Phi_0} Byd. \tag{48}$$

It is important to note here that $\phi_2 - \phi_1$ is defined deep within the respective super-conductors, and is thus single-valued across the whole junction.

To obtain the supercurrent density flowing across the gap, Equation 48 can be plugged into Equation 42, the first Josephson relation, to yield

$$j_s = j_c \sin\left(\gamma_0 + \frac{2\pi}{\Phi_0} Byd\right), \tag{49}$$

where the total current I_s has been replaced with the current density j_s. It is therefore evident that, for a straight-walled Josephson junction in a uniform magnetic field, the gauge invariant phase increases linearly along the junction, causing the supercurrent
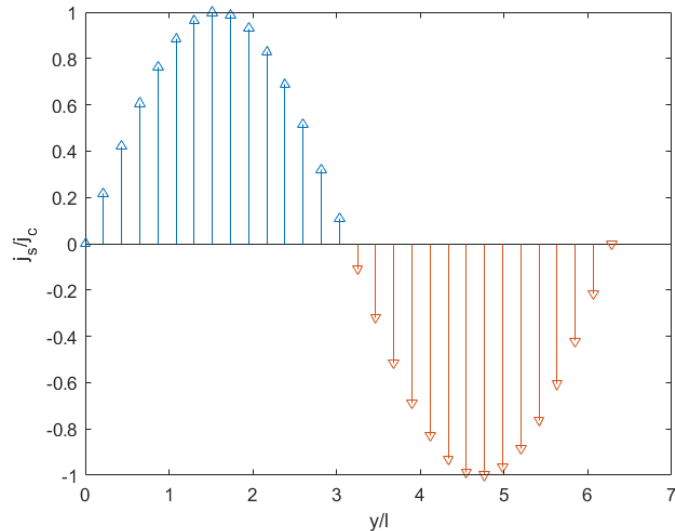
to oscillate sinusoidally, as shown in Figure 8.

Figure 8. Supercurrent density flowing across a straight-walled Josephson junction. γ_0 was chosen to be zero and the magnetic field strength was chosen such that there is exactly one flux quanta contained in the gap.

The locations along the gap where j_s goes to zero are known as Josephson vortices. Importantly, these vortices have the ability to bind Majorana zero modes, so knowledge of the vortex locations also constitutes knowledge of the locations of the Majorana in the system (18). Because the gauge invariant phase can be manipulated in time by an applied voltage according to Equation 43, the locations of these vortices can be effectively controlled. This is useful for the manipulation of states via exchange, as the vortices could potentially be moved around each other in a lattice of Josephson junctions.

III. Methodology and Results

3.1 Vortex Locations for Arbitrarily Shaped Junction

It may not be possible to always manufacture perfectly straight Josephson junctions for any particular arrangement; therefore, it is important to be able to predict where the Majorana-hosting Josephson vortices will form for an arbitrarily shaped Josephson junction. Consider a junction like the one shown in Figure 9, where the width of the junction is given by a function $w(y)$. The magnetic field is still oriented
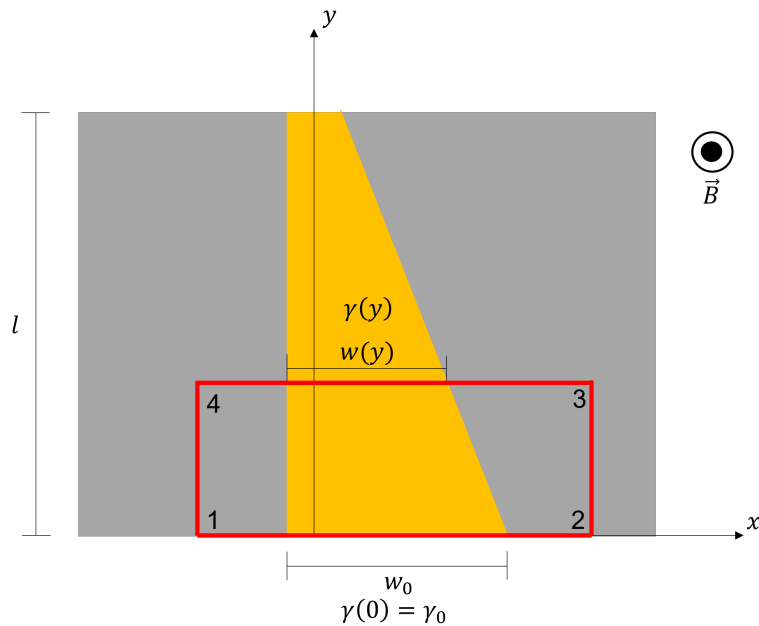

Figure 9. A Josephson junction of arbitrary shape. The distance between the superconductors at any distance y in the junction is given by w(y).

perpendicular to the plane, and the gauge invariant phase at any point in the junction $\gamma(y)$ is determined by the shape of the Josephson junction.

Since the magnetic field is screened to zero inside the superconductors, the flux through the highlighted area is given by the integration of $w(y)$ from the zero to y

multiplied by the field strength, and is related to the vector potential by

$$\Phi = B \int_0^y w(y)dy = \oint \vec{A} \cdot d\vec{s}. \tag{50}$$

Choosing the gauge $A_x = -By$ and $A_y = 0$ as was done for the straight junction allows for the integral along path $1 \to 2$ to be elimated, with the integrals along paths $2 \to 3$ and $4 \to 1$ being eliminated if the contours are chosen to be farther into the superconductors than the London penetration depth. Because of this, the integration of the vector potential across the Josephson junction at any value y is equal to the flux contained by the junction to that point. In other words,

$$\int_3^4 \vec{A} \cdot d\vec{s} = B \int_0^y w(y)dy. \tag{51}$$

The integral across the junction in Equation 41 can then be replaced by the flux, so that $\gamma(y)$ is given by

$$\gamma(y) = \phi_2 - \phi_1 + \frac{2\pi}{\Phi_0} \int_0^y w(y)dy. \tag{52}$$

As with the straight junction, $\phi_2 - \phi_1$ is considered deep into the superconductors so that it is single-valued throughout the junction. This consideration, along with the choice of gauge, means $\phi_2 - \phi_1 = \gamma(0) = \gamma_0$, which finalizes the expression for $\gamma(y)$ in an arbitrarily shaped junction to

$$\gamma(y) = \gamma_0 + \frac{2\pi}{\Phi_0} \int_0^y w(y)dy = \gamma_0 + 2\pi \frac{\Phi}{\Phi_0}. \tag{53}$$

In most cases, the system will relax to the ground state in which no net supercurrent flows between the islands, meaning $\gamma_0 = 0$. Locations in the junction where $|\gamma(y) - \gamma_0| = n\pi$ correspond to the location of a vortex.

The following figures are computationally generated examples of how this expres-

sion can be implemented to find vortex locations for various junction shapes. In each of these figures, the superconducting islands were assumed to be approximately 600 nm long, with the Josephson junction being on the order of 100 nm wide. The magnetic field strength was set to 0.02 T, and the integration was performed trapezoidally with a step size of approximately 1 nm. Additionally, γ_0 was assumed to be zero at the bottom of all the junctions. Figure 10 shows a junction which is straight on one side and linearly sloping on the other. The junction in Figure 11 is linearly sloped on one side, but follows the shape of a sine curve on the other side. Finally, Figure 12 displays a junction where each side consists of a random walk in order to simulate a more jagged junction.
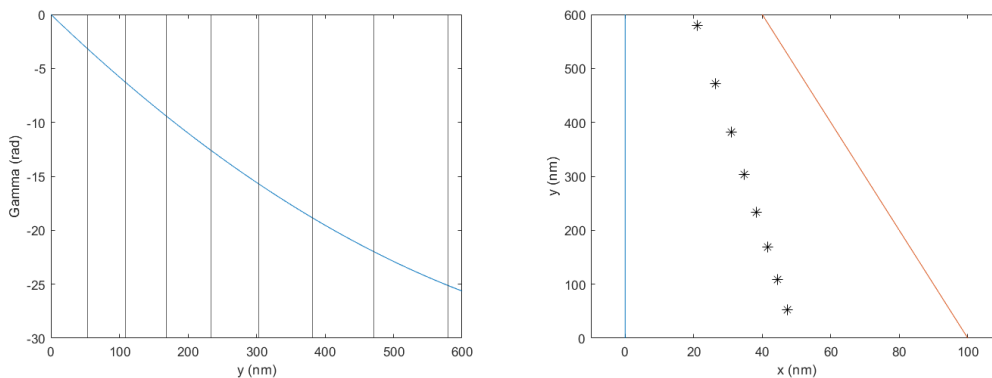

Figure 10. Vortex locations for a sloped junction. The plot on the left shows γ as a function of y. The vertical lines indicate where γ has changed by π, and thus represents the location of a vortex. The plot on the right shows a depiction of the junction, with the blue line indicating the left side of the junction, the orange line indicating the right side, and the asterisks representing vortex locations. Note how as the junction narrows, the vortices become more spread out.

This technique can also be applied outside of computer simulations. For instance, if an image of a manufactured Josephson junction is taken in a lab, and a file containing values for the width across the junction is generated from it, this method can be used to predict where vortices will form in the junction.
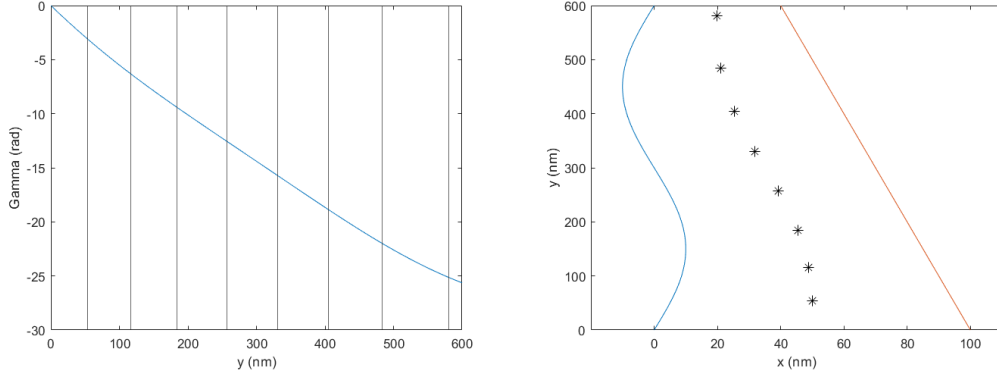
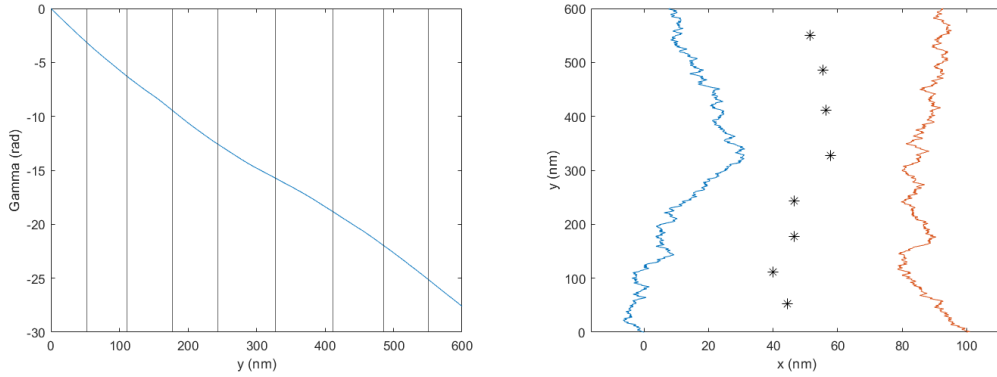**Figure 11.** Vortex locations for a junction with one side shaped sinusoidally and the other sloped.

Figure 12. Vortex locations for a junction where each side consists of a random walk, simulating a more jagged junction.

3.2 Vortex Locations in a 2x2 Array of Superconducting Islands

Consider now a 2x2 array of superconducting islands on a topological insulator, as shown in Figure 13. This setup contains four junctions where Josephson vortices can form and one intersection where Abrikosov vortices can form.

Since the location of γ_0 for each junction is arbitrary, it can be defined to be along the inside edge of each junction, so γ_2, γ_3, γ_5, and γ_8 represent γ_0 for their respective junctions. In accordance with the derivation for a single junction, γ_0 is equal to the
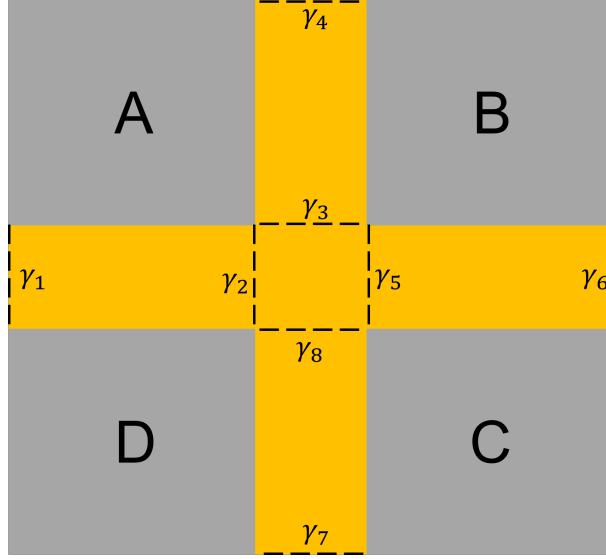
Figure 13. A series of Josephson junctions formed by a 2x2 array of superconducting islands. The superconductors are represented by the gray areas and labeled A-D. The exposed topological insulator is shown in orange.

overall phase difference between the islands, so

$$\gamma_2 = \phi_A - \phi_D, \tag{54}$$

$$\gamma_3 = \phi_B - \phi_A, \tag{55}$$

$$\gamma_5 = \phi_B - \phi_C, \tag{56}$$

$$\gamma_8 = \phi_C - \phi_D. \tag{57}$$

Note that γ_i has been defined to be positive upward and to the right. The sum around the inner contour is related to the number of flux quanta f contained by the intersection and the number of Abrikosov vortices n by (17)

$$\sum_{plaquette} \gamma_i = \gamma_5 - \gamma_3 - \gamma_2 + \gamma_8 = 2\pi(f - n), \tag{58}$$

where the summation of γ_i is taken along the inside plaquette that outlines the in-

26

tersection. This summation is taken in a circular sense, with positive defined as counterclockwise, and hence γ_3 and γ_2 are subtracted instead of added. Note that a positive value of n indicates a vortex, while a negative n indicates an antivortex.

To find the ground state of the system, it is necessary to find the minimum energy contained by the array. The energy of a superconducting island array consisting of point junctions is given by (17)

$$E = E_J \sum_{array} (1 - \cos \gamma_i), \tag{59}$$

where E_j is the single-junction energy.

While a good starting point, this expression does not adequately describe the array shown in Figure 13, as the junctions are not point junctions and therefore cannot be characterized by a single value of γ. Instead, the energy of the array will be given by summing the integrals of all junctions. Equation 59 becomes

$$E = E_J \sum_{array} \int [1 - \cos(\gamma_i(y))] \, dy, \tag{60}$$

where the integral is taken along each junction from the intersection outwards. If the junctions are all said to be perfectly straight junctions of the same size, Equation 59 can be integrated to the form

$$E = \frac{E_J \Phi_0}{2\pi B d} \sum_{array} \left(\frac{2\pi B dw}{\Phi_0} - \sin\left(\gamma_{0,i} + \frac{2\pi}{\Phi_0} B dw \right) - \sin(\gamma_{0,i}) \right), \tag{61}$$

where B is the magnetic field strength, w is the width of one superconducting island, and d is the separation between islands. If the junctions are not identical straight junctions, numerical integration of Equation 53 can be used to compute the energy. Minimization of Equation 61 with respect to $\gamma_{0,i}$ will yield the ground state of the

system; however, $\gamma_{0,i}$ is constrained by Equation 58, as the number of Abrikosov vortices must be an integer value.

The minimum energy will come when $|\gamma_{0,i}|$ is equal for all junctions, with $\gamma_{0,i}$ for junctions AB and DA of opposite sign to junctions DC and CB. This allows for the energy to be expressed in terms of a single variable γ_0. Using this, Equation 61 and Equation 58 become

$$E = \frac{4E_J\Phi_0}{2\pi Bd}\left[\frac{2\pi Bdw}{\Phi_0} - \sin\left(\frac{2\pi}{\Phi_0}Bdw\right)\cos(\gamma_0)\right],\tag{62}$$

and

$$\gamma_0 = \frac{\pi}{2}(f - n).\tag{63}$$

These can now be combined to find E as a function of n. This yields

$$E = \frac{4E_J\Phi_0}{2\pi Bd}\left[\frac{2\pi Bdw}{\Phi_0} - \sin\left(\frac{2\pi}{\Phi_0}Bdw\right)\cos\left(\frac{\pi}{2}(f - n)\right)\right].\tag{64}$$

The simplest way of finding the value for n that generates the minimum energy is to do so graphically. Figure 14 shows a plot of E/E_J for several values of n, ranging from -10 to 10. This plot was for an array with islands 300 nm long, a separation of 50 nm, and a magnetic field of 0.1 T. The ground state of the array will correspond to the minimum number of Abrikosov vortices or antivortices that minimize the energy of the overall array. In the case illustrated, this is $n = \pm2$, which corresponds to a superposition of two vortices and two antivortices. It can be seen that the plot is periodic with a period of 4, so the only case that will result in a superposition is the case where $|n| = 2$. $n = 0, \pm1$ will be definitively in that state.

The number of Abrikosov vortices that define the ground state will evolve as the magnetic field strength is increased. This is shown in Figure 15. Interestingly, as the fractional flux quanta f through the intersection increases, the number of vortices
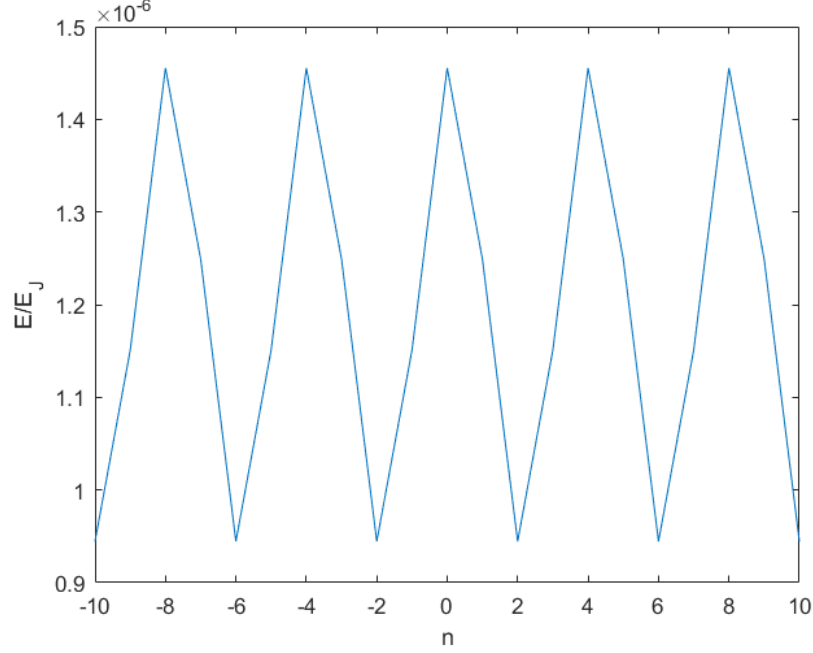
Figure 14. Graphical determination of n, the number of Abrikosov vortices in the intersection of the array. The ground state of the system corresponds to the minimum amount of Abrikosov vortices or antivortices that minimize the total energy of the array. The plot shows that n can be either 2 or -2 for this configuration.

alternates between ± 2 and 0. However, at $f = 0.5$ this alternation switches to be between -1 and 1, and then switches back at $f = 1.5$.

Once the ideal value for n has been found, γ_0 is found using Equation 63. From there, the value of $\gamma(y)$ within each junction is completely predetermined by the geometry of each junction. For the same straight-walled array described above with a magnetic field of 0.29 T, Figure 16 shows the current distribution across each junction. In this case, $n = 0$ and the current flows clockwise around the innermost loop. It can be seen that the current density along each junction crosses zero four times, corresponding to four Josephson vortices. Therefore, this configuration contains a total of 16 Josephson vortices and zero Abrikosov vortices. A complete illustration of this array is given in Figure 17.

Increasing the magnetic field strength will force the system into a state with
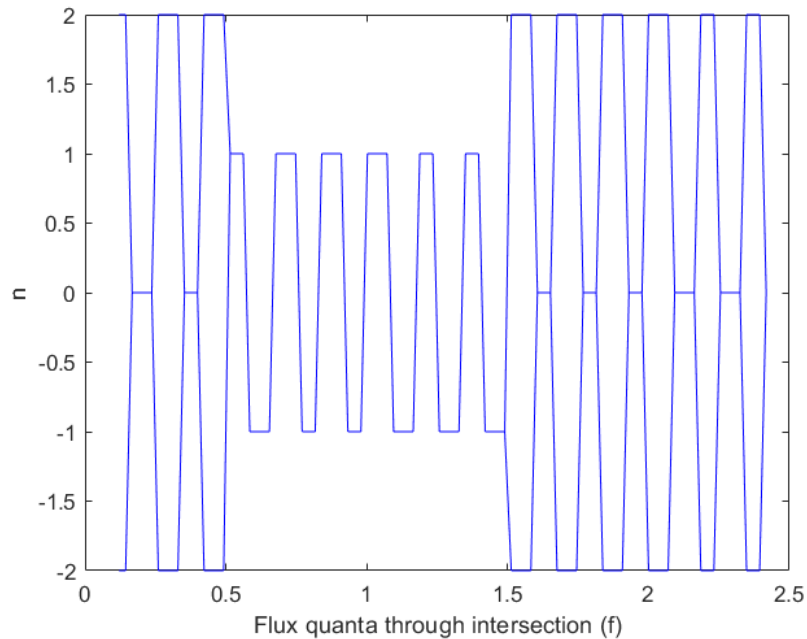
Figure 15. n **as a function of flux quanta** f **through the intersection of the array. Places where** n **can be** ± 2 **are plotted as both 2 and** -2**. Note that at half-integer values of** f**,** n **goes from switching between 0 and** ± 2 **to switching between 1 and** -1**.**

$|n| = 1$ Abrikosov vortex, as shown in Figure 18.

While it is certainly possible to continue to increase the field strength, once the number of fractional flux quanta through the intersection starts to exceed 1, the number of Josephson vortices starts to get unruly. For example, given $f = 1.14$, each junction would contain 13 Josephson vortices, for a total of 52 in the entire array. Expand this to a larger array, i.e. 3x3, 4x4, or larger, and the total number of Josephson vortices quickly gets to be out of hand. Therefore, it is beneficial to keep f below 1.

Using the concepts introduced here, it is possible to predict exactly where the vortices will form in any 2x2 array of superconducting islands. Even if the junctions are not perfectly straight, by presenting a solution for an arbitrarily-shaped junction, the array can still be solved using Equation 53. The code used to generate Figure 14 through Figure 18 has been included in Appendix A. It should be straightforward to
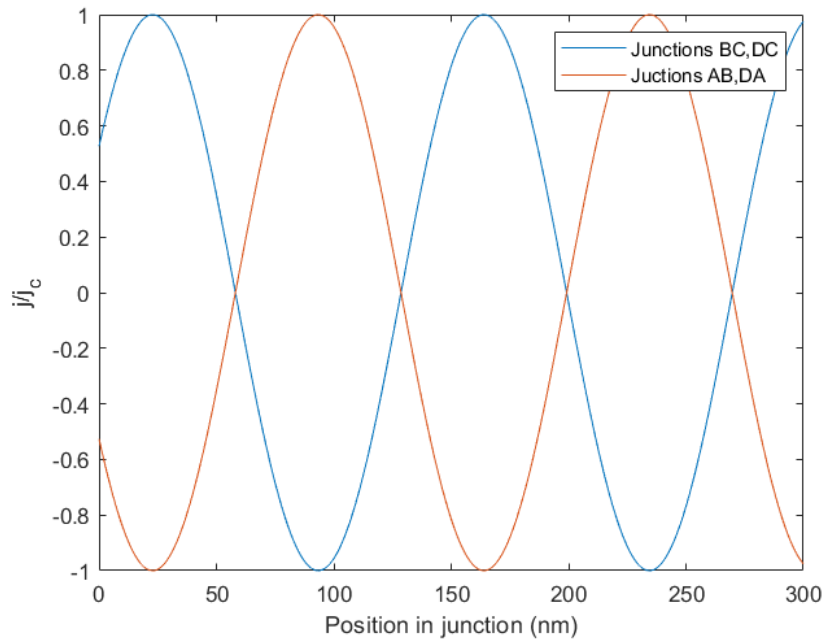
Figure 16. Current as a function of y in each junction. Note how the currents across junctions AB and DA are in the opposite direction of those in junctions DC and BC.

apply the same method of energy minimization used here to a larger array for future implementations, although an array with more than one intersection will be slightly more complex, as the value of γ_0 for one intersection will impact the value for its conjugate.
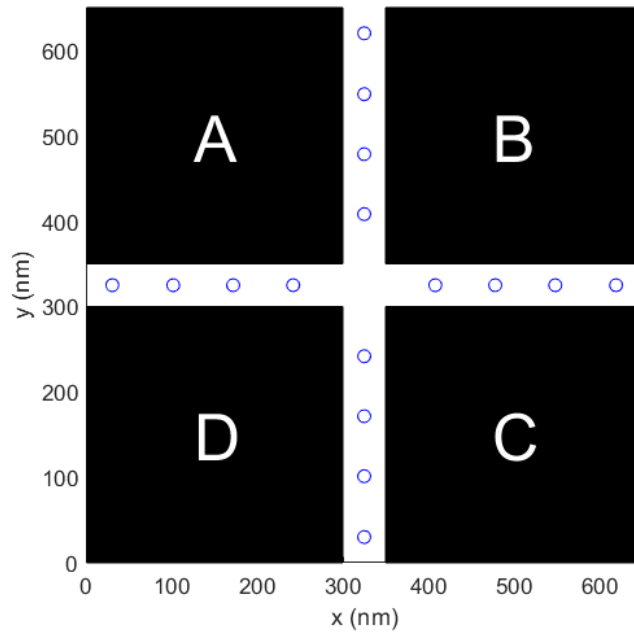
Figure 17. An illustration of an array with island width of 300 nm, separation of 50 nm, and magnetic field strength of 0.29 T, which corresponds to $f = 0.35$. Josephson vortices are given in blue and there are no Abrikosov vortices present.
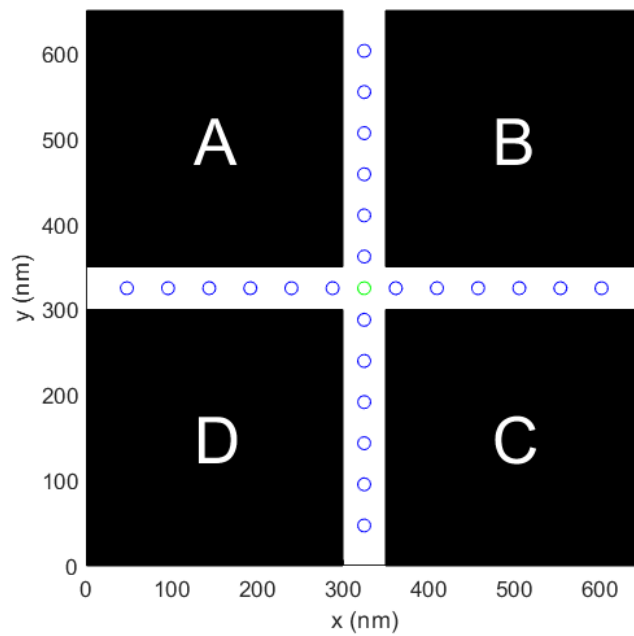

Figure 18. Island array with magnetic field strength of 0.43 T, corresponding to $f = 0.52$. Six Josephson vortices (blue) are present along with one Abrikosov vortex (green).

IV. Conclusions

Majorana-based qubits are promising theoretical candidates for error-free quantum computation. Their topological protection and non-abelian exchange statistics allow for easy state manipulation while minimizing decoherence due to local perturbations from the environment. One potential manner to construct a Majorana-based qubit exists in the form of a superconducting island array on top of a topological insulator, where superconductivity in the insulator is induced by the surrounding islands. In this setup, the Majorana fermions are hosted in Josephson and Abrikosov vortices found in the gaps between islands and can be manipulated by applied voltages between islands. However, little is currently known about such systems.

Practical implementation of Majorana-based qubits requires knowledge of where the Majorana-hosting vortices will form. This work helps advance this knowledge in two ways. First, a method for determining Josephson vortex locations was presented for a Josephson junction of arbitrary shape. This will allow for more accurate vortex location knowledge in a physical system after it has been constructed. Second, a 2x2 superconducting island array was analyzed for Abrikosov and Josephson vortex locations. This solution minimizes the energy of the array by relating the gauge invariant phase for each junction at the center of the array with the magnetic flux through the intersection and the number of Abrikosov vortices. Due to system constraints, the variable that must be analyzed to minimize the energy is the number of Abrikosov vortices. Once this number is found, the gauge invariant phase for each junction is determined, with the locations of the Josephson vortices being predetermined by the geometry of the junctions. These two advances are complementary and can be used in conjunction with each other for physical arrays of irregularly-shaped islands.

Future work in this field could involve altering the arbitrarily-shaped junction solution to include variation in the critical current density as the distance across the

junction increases. This would involve a deeper understanding of the constant K that couples the wavefunctions of the two superconductors together. Additionally, work could be done to expand the array, first to a 3x2 array to investigate the effect of adding another intersection, then to a larger array that will allow for actual exchange of vortices. Finally, the dynamics of the array could be investigated for an applied voltage between islands with the end goal of being able to move the vortices around each other.

Appendix A. MatLab Code for Array Analysis

```matlab
1  clc
2  clear all
3  close all
4
5  d = 50e-9;%separation
6  w = 300e-9;%island length
7  B = .8*10e-2; %Magnetic field strength, in tesla
8
9  dy = 1e-9; %resolution of microscope in m
10 sep = d; %approximate separation of islands
11 ht = w; %approximate length of islands
12 num = round(ht/dy); %number of distance entries
13 y = transpose(linspace(0,ht,num)); %linearly spaced y values
14 chg = 1.602e-19; %electron charge
15 hbar = 1.05e-34; %h bar
16 flux = zeros(num,1);
17 phi0 = 6.626e-34/2/1.602e-19;
18 x = linspace(0,w,num);
19
20
21 f = d^2*B/phi0; %fractional flux through intersection
22 g = d*w*B/phi0; %fractional flux through junction
23
24 flux = linspace(0,w*d*B,num);
25
26 B_mat = 10e-2*linspace(1,20,100);
27 f = d^2*B/phi0; %fractional flux through intersection
28 n_opts = zeros(size(B_mat));
```

```matlab
29  fmat = d^2*B_mat/phi0;

30

31  figure
32  for ii=1:length(B_mat)
33      B = B_mat(ii);
34      f = d^2*B/phi0;
35      ns = [-3:1:3];
36      E = 4*phi0/(2*pi*B*d)*(2*pi*B*d*w/phi0 - ...
            sin(2*pi/phi0*B*d*w)*cos(pi/2*(f-ns)));
37      [M,I] = min(E);
38      indices = find(E==M,20);
39      %Ind = min(abs(indices-(length(ns)-1)/2)) + (length(ns)-1)/2
40      %[Min,Ind] = min(abs(ns(indices)));
41      Ref = (length(ns)-1)/2+1;
42      Diff = abs(indices - Ref);
43      [minVal, minInd] = min(Diff);
44      Ind = indices(minInd);
45      n_opts(ii) = ns(Ind);
46      ns(Ind);
47      plot(ns,E)
48      xlabel('n')
49      ylabel('E/E_J')
50      hold on
51  end
52  n_opts_2 = find(n_opts==-2);
53  n_opts_sup = n_opts;
54  n_opts_sup(n_opts_2) = 2;

55

56

57  figure
58  plot(fmat,n_opts,'b')
59  xlabel('Flux quanta through intersection (f)')
```

```matlab
60  ylabel('n')
61  hold on
62  plot(fmat,n_opts_sup,'b')
63
64  reference_num = 18;
65  gam0s = pi/2*(fmat-n_opts);
66  flux = linspace(0,w*d*B_mat(reference_num),num);
67  gamBC = gam0s(reference_num) + 2*chg/hbar*flux;
68  gamAB = -gam0s(reference_num) - 2*chg/hbar*flux;
69  figure
70  plot(x/1e-9,sin(gamBC))
71  hold on
72  plot(x/1e-9,sin(gamAB))
73  xlabel('Position in junction (nm)')
74  ylabel('j/j_c')
75  n = n_opts(reference_num)
76  legend('Junctions BC,DC','Juctions AB,DA')
77
78  gamDA = gamAB;
79  gamDC = gamBC;
80
81  [num_vorticesAB_3 vort_indexAB_3] = FindZeros(sin(gamAB));
82  [num_vorticesBC_3 vort_indexBC_3] = FindZeros(sin(gamBC));
83  [num_vorticesDA_3 vort_indexDA_3] = FindZeros(sin(gamDA));
84  [num_vorticesDC_3 vort_indexDC_3] = FindZeros(sin(gamDC));
85
86  vorticesAB = y(vort_indexAB_3); %how far in nm into the junction the ...
        vortices are located
87  vorticesDA = y(vort_indexDA_3);
88  vorticesBC = y(vort_indexBC_3);
89  vorticesDC = y(vort_indexDC_3);
90
```

```matlab
91  vert_junc_x_coord = w+d/2;

92  horz_junc_y_coord = w+d/2;

93  vorticesAB_y_coord = vorticesAB + w+d;

94  vorticesDC_y_coord = w - vorticesDC;

95  vorticesDA_x_coord = w - vorticesDA;

96  vorticesBC_x_coord = vorticesDC + w+d;

97

98  vorticesAB_coords = [zeros(length(vorticesAB),1)+vert_junc_x_coord, ...
        vorticesAB_y_coord];

99  vorticesDC_coords = [zeros(length(vorticesDC),1)+vert_junc_x_coord, ...
        vorticesDC_y_coord];

100 vorticesDA_coords = [vorticesDA_x_coord, ...
        zeros(length(vorticesDA),1)+horz_junc_y_coord];

101 vorticesBC_coords = [vorticesBC_x_coord, ...
        zeros(length(vorticesBC),1)+horz_junc_y_coord];

102

103 figure

104 rectangle('position',[0 0 w w]/1e-9,'FaceColor','black')

105 hold on

106 rectangle('position',[w+d 0 w w]/1e-9,'FaceColor','black')

107 rectangle('position',[0 w+d w w]/1e-9,'FaceColor','black')

108 rectangle('position',[w+d w+d w w]/1e-9,'FaceColor','black')

109 axis image

110 plot(vorticesAB_coords(:,1)/1e-9,vorticesAB_coords(:,2)/1e-9,'bo')

111 plot(vorticesDC_coords(:,1)/1e-9,vorticesDC_coords(:,2)/1e-9,'bo')

112 plot(vorticesDA_coords(:,1)/1e-9,vorticesDA_coords(:,2)/1e-9,'bo')

113 plot(vorticesBC_coords(:,1)/1e-9,vorticesBC_coords(:,2)/1e-9,'bo')

114

115 if n == 1

116     plot((w+d/2)/1e-9,(w+d/2)/1e-9,'go')

117 elseif n == -1

118     plot((w+d/2)/1e-9,(w+d/2)/1e-9,'ro')
```

```matlab
119  elseif n ==  2
120      plot((w+d/2-5)/1e-9,(w+d/2)/1e-9,'go')
121      plot((w+d/2+5)/1e-9,(w+d/2)/1e-9,'go')
122  elseif n == -2
123      plot((w+d/2-5)/1e-9,(w+d/2)/1e-9,'ro')
124      plot((w+d/2+5)/1e-9,(w+d/2)/1e-9,'ro')
125  end
126  xlabel('x (nm)')
127  ylabel('y (nm)')
128
129  tA = ...
         text((w/2-d/2)/1e-9,(w/2+w/2+w/2+d)/1e-9,'A','Color','white','FontSize',30);
130  tB = ...
         text((w/2+w+d/2)/1e-9,(w/2+w/2+w/2+d)/1e-9,'B','Color','white','FontSize',30);
131  tC = ...
         text((w/2+w+d/2)/1e-9,(w/2)/1e-9,'C','Color','white','FontSize',30);
132  tB = text((w/2-d/2)/1e-9,(w/2)/1e-9,'D','Color','white','FontSize',30);
133
134  function [n,z_indices] = FindZeros(array) %must be large array with ...
         no noise
135  abs_array = abs(array);
136  n = 0;
137  z_indices = [];
138  for ii = 2:length(array)-1
139      if abs_array(ii-1) > abs_array(ii) && abs_array(ii+1) > ...
             abs_array(ii)
140          n = n+1;
141          z_indices = [z_indices ii];
142      end
143  end
144  end
145  end
```

Bibliography

1. E. Martin-Lopez, A. Laing, T. Lawson, R. Alvarez, X.-Q. Zhou, and J. L. O'brien, "Experimental realization of shor's quantum factoring algorithm using qubit recycling," *Nature photonics*, vol. 6, no. 11, pp. 773–776, 2012.

2. D. P. DiVincenzo, "The physical implementation of quantum computation," *Fortschritte der Physik: Progress of Physics*, vol. 48, no. 9-11, pp. 771–783, 2000.

3. S. R. Lee, P. A. Sharma, A. L. Lima-Sharma, W. Pan, and T. M. Nenoff, "Topological quantum materials for realizing majorana quasiparticles," *Chemistry of Materials*, vol. 31, no. 1, pp. 26–51, 2018.

4. F. London and H. London, "The electromagnetic equations of the supraconductor," *Proceedings of the Royal Society of London. Series A-Mathematical and Physical Sciences*, vol. 149, no. 866, pp. 71–88, 1935.

5. H. Eschrig, "Theory of superconductivity a primer," 2001.

6. S. D. Sarma, M. Freedman, and C. Nayak, "Majorana zero modes and topological quantum computation," *npj Quantum Information*, vol. 1, no. 1, pp. 1–13, 2015.

7. M. Leijnse and K. Flensberg, "Introduction to topological superconductivity and majorana fermions," *Semiconductor Science and Technology*, vol. 27, no. 12, p. 124003, 2012.

8. R. Akzyanov, A. Rozhkov, A. Rakhmanov, and F. Nori, "Tunneling spectrum of a pinned vortex with a robust majorana state," *Physical Review B*, vol. 89, no. 8, p. 085409, 2014.

9. J. D. Sau, R. M. Lutchyn, S. Tewari, and S. D. Sarma, "Robustness of majorana fermions in proximity-induced superconductors," *Physical Review B*, vol. 82, no. 9, p. 094522, 2010.

10. S. Rao, "Introduction to abelian and non-abelian anyons," in *Topology and Condensed Matter Physics*, pp. 399–437, Springer, 2017.

11. L. S. Georgiev, "Topologically protected gates for quantum computation with non-abelian anyons in the pfaffian quantum hall state," *Physical Review B*, vol. 74, no. 23, p. 235112, 2006.

12. F. Hassler, A. Akhmerov, C. Hou, and C. Beenakker, "Anyonic interferometry without anyons: how a flux qubit can read out a topological qubit," *New Journal of Physics*, vol. 12, no. 12, p. 125002, 2010.

13. B. D. Josephson, "Possible new effects in superconductive tunnelling," *Physics Letters*, vol. 1, pp. 251–253, July 1962.

14. B. D. Josephson, "The discovery of tunnelling supercurrents," *Reviews of Modern Physics*, vol. 46, no. 2, p. 251, 1974.

15. A. Kraft, C. Rupprecht, and Y.-C. Yam, "Superconducting quantum interference device (squid)," 2017.

16. P. Krantz, M. Kjaergaard, F. Yan, T. P. Orlando, S. Gustavsson, and W. D. Oliver, "A quantum engineer's guide to superconducting qubits," *Applied Physics Reviews*, vol. 6, no. 2, p. 021318, 2019.

17. M. Tinkham, *Introduction to superconductivity.* Courier Corporation, 2004.

18. E. Grosfeld and A. Stern, "Observing majorana bound states of josephson vortices

in topological superconductors," *Proceedings of the National Academy of Sciences*, vol. 108, no. 29, pp. 11810–11814, 2011.

REPORT DOCUMENTATION PAGE

Form Approved
OMB No. 0704–0188

1. REPORT DATE *(DD–MM–YYYY)*	2. REPORT TYPE	3. DATES COVERED *(From — To)*
21–03–2022	Master's Thesis	Jun 2020 — Mar 2022

4. TITLE AND SUBTITLE

DETERMINATION OF VORTEX LOCATIONS IN A 2X2 JOSEPHSON JUNCTION ARRAY FOR TOPOLOGICAL QUANTUM COMPUTATION

5a. CONTRACT NUMBER

5b. GRANT NUMBER

5c. PROGRAM ELEMENT NUMBER

6. AUTHOR(S)

Kowalski, Casey Lorenz, 2d Lt, USAF

5d. PROJECT NUMBER

5e. TASK NUMBER

5f. WORK UNIT NUMBER

7. PERFORMING ORGANIZATION NAME(S) AND ADDRESS(ES)

Air Force Institute of Technology
Graduate School of Engineering and Management (AFIT/EN)
2950 Hobson Way
WPAFB OH 45433-7765

8. PERFORMING ORGANIZATION REPORT NUMBER

AFIT-ENP-MS-22-M-099

9. SPONSORING / MONITORING AGENCY NAME(S) AND ADDRESS(ES)

10. SPONSOR/MONITOR'S ACRONYM(S)

11. SPONSOR/MONITOR'S REPORT NUMBER(S)

12. DISTRIBUTION / AVAILABILITY STATEMENT

DISTRIBUTION STATEMENT A:
APPROVED FOR PUBLIC RELEASE; DISTRIBUTION UNLIMITED.

13. SUPPLEMENTARY NOTES

14. ABSTRACT

A large barrier to practical quantum computation exists in the form of qubit decoherence, which leads to high noise and error when implementing quantum algorithms. A potential solution to this problem is the use of topologically-protected Majorana-based qubits, as their nonlocal nature and unique non-abelian exchange statistics render them virtually immune to decoherence while still allowing the state to be easily manipulated. For such a qubit to be constructed, it is essential to know the locations of the Majorana-hosting vortices in the system. This work presents a solution for the formation locations of vortices in a 2x2 superconducting island array, paving the way for the analysis of larger arrays that allow for the physical exchange of particles. Additionally, a method for determining the vortex locations in an irregularly-shaped Josephson junction is derived, allowing for accurate predictions of Majorana fermion locations in manufactured systems where the junctions may not be perfectly straight.

15. SUBJECT TERMS

Quantum Computing, Topological Qubits, Majorana, Josephson Junction, Superconducting Island Array

16. SECURITY CLASSIFICATION OF:			17. LIMITATION OF ABSTRACT	18. NUMBER OF PAGES	19a. NAME OF RESPONSIBLE PERSON
a. REPORT	b. ABSTRACT	c. THIS PAGE			Dr. Michael V Pak, AFIT/ENP
U	U	U	U	42	19b. TELEPHONE NUMBER *(include area code)* (937) 255-3636; Michael.Pak@afit.edu

Standard Form 298 (Rev. 8–98)
Prescribed by ANSI Std. Z39.18